Proceedings of the 11th World Congress on Mechanical, Chemical, and Material Engineering (MCM'25)

Paris, France - August, 2025 Paper No. ICMIE 190 DOI: 10.11159/icmie25.190

A Comparative Thermo-Mechanical Reverse-Flow-Forming Analysis on High Strength Alloys: A DOE-Based Numerical Study

Gokul Vikraman¹, Ajith Ramesh^{1*}, Venkataraman Balasubramanian¹

¹Department of Mechanical Engineering, Amrita School of Engineering, Coimbatore, Amrita Vishwa Vidyapeetham, India v gokul@cb.students.amrita.edu; r ajith@cb.amrita.edu; b venkataraman@cb.amrita.edu

Abstract - Flow-forming is a highly precise metal forming process extensively used in aerospace and defence sectors for manufacturing high strength, thin-walled tubular components. In the presented research, a detailed finite element (FE) thermo-mechanical model using Abaqus/Explicit is developed to investigate the influence of key process parameters on the structural integrity of the flow-formed tubes. This study evaluates three different types of alloys, Maraging Steel – 250 (MDN 250), 15CDV6, and AISI 4130. These materials are selected due to their widespread use in flow-forming applications pertaining to aerospace and defence sectors. The use of flow-forming on these materials enhance mechanical properties through work hardening, ensures precise dimensional control, and reduces material wastage, making them optimal choices for thin-walled tubular components in critical applications, A Taguchi L9 orthogonal array is utilized to systematically analyse the influence of process parameter in feed ratio, percentage reduction, and axial stagger, and their effects are analysed on critical dimensional outcomes such as ovality, diametral growth, and spring-back. Additionally, thermo-structural response outputs like equivalent plastic strain (PEEQ) and temperature distribution at the roller-preform interface are monitored to evaluate the severity of these effects across the three materials. The results indicate a strong correlation between input parameters and PEEQ, with higher strain levels leading to an increased risk of defects and potential onset of failures. Significant thermal gradients are observed as the rollers engage with the preform, with peak temperatures localized at the contact zone due to frictional heating. This localized temperature rise contributes to material softening, thereby, promoting relevant plastic flow and an improved surface conformity. These insights provide a valuable basis for understanding materialprocess interactions and optimizing flow-forming conditions to enhance dimensional precision with minimal defects.

Keywords: Flow-forming; incremental metal forming; spring-back; diametral growth; ovality; Taguchi method

1. Introduction

Flow-forming has emerged as a critical manufacturing process for producing thin-walled, high-strength tubular components, particularly in sectors where part precision and structural integrity are paramount factors i.e., aerospace, defence and space propulsion [1], [2], [3]. It is an incremental forming process wherein the preform is gradually shaped into a seamless tube through successive local deformations. This is achieved by one or more rollers exerting pressure on the preform attached to a rotating mandrel, causing plastic flow that reduces wall thickness and increases the tube length. Compared to conventional methods, flow forming offers significant advantages in terms of material efficiency, dimensional accuracy, and mechanical strength due to work hardening.

Researchers investigated the influence of key process parameters—such as feed rate, mandrel speed, and roller in-feed on the out-of-roundness of annealed and flow-formed AISI 321 steel tubular preforms using Taguchi's orthogonal array design. Their study revealed that mandrel speed had the most significant effect on dimensional accuracy, with lower speeds reducing the deviation from roundness due to more uniform plastic deformation [4]. Accompanying this, there were studies carried out experimental optimization of flow forming parameters for AA6082 tubes with the goal of minimizing surface roughness. Using Design of Experiments (DOE), they found that roller speed and feed rate critically influenced surface quality, with optimal conditions producing a uniform and smooth surface finish [5]. Both studies underscore the importance of statistically guided parameter selection in improving flow forming outcomes, highlighting how variations in forming conditions can significantly impact the final product geometry and surface integrity.

There were studies which employed an explicit finite element software to model the forward flow forming process of tubes and established a relationship linking the feed rate with both axial and angular velocities [6]. The effects of process

parameters such as axial stagger, feed ratio, and percentage reduction on key outcomes like ovality, diametral growth, and spring-back on single pass and multi-pass scenarios were studied [7]. The results indicate that multi-pass flow forming provides a more favourable response of input parameters on part accuracy compared to single-pass forming, enabling improved control over output parameters. Experimental investigations were conducted to evaluate how heat treatment of the preform influences the mechanical properties of flow-formed AISI 4130 steel tubes. The research also explains the estimation of preform dimensions based on the final formed tube according to the user's applications [8]. In this procedure for estimating the preform dimensions there are other factors also to be considered. To overcome these challenges, in the current study the developed thermo-mechanical finite element (FE) model serves as a powerful tool for analysing the process mechanics and optimizing the input parameters.

Experimental investigations are often time-consuming, costly, and limited in their ability to provide a detailed insight into field variables such as strain distribution, temperature rise etc. Therefore, integrating experimental insights with robust finite element simulations not only enhances our understanding of the intricate deformation mechanisms in flow forming but also enables cost-effective optimization of process parameters.

2. Geometric Modelling and Simulation Setup

A three-dimensional thermo-mechanical flow-forming model was developed using Abaqus/Explicit to simulate the deformation behaviour of a tubular preform. The overall geometry of the setup, including the preform, mandrel, and rollers, is adapted from existing literature to reflect realistic process conditions and to enable comparison with validated benchmarks [9]. The model comprises a deformable preform and three staggered rollers interacting with a rigid mandrel, as illustrated in Figure 1a. The preform, with an inner diameter of 222 mm and wall thickness of 12 mm, is modelled as a deformable body, while the mandrel and rollers are defined as analytical rigid bodies to reduce computational cost.

Three rollers, each with a radius of 132 mm, are employed in the setup. These rollers are axially staggered and differ in geometric features such as attack angle, nose radius, and relief angle is modelled based on the reference paper and depicted in Figure 1b. For visual reference, Roller Z is shown in grey, Roller Y in blue, and Roller X in red. The schematic diagram of the rollers is shown in Figure 1c. The rollers are also circumferentially staggered at 120° intervals around the preform, as shown in Figure 1d.

The preform is meshed using C3D8RT elements—eight-nodded brick elements with reduced integration and temperature-displacement degrees of freedom—to capture the thermo-mechanical behaviour accurately. A kinematic inversion strategy is employed in the simulation, i.e., the preform is held stationary while the rollers which rotate passively about their axes, also revolve around the preform, in addition to executing an axial translation. This contrasts with the actual experimental configuration, where the preform rotates with the mandrel and the rollers execute only axial movement. The kinematic inversion technique accurately replicates the relative motion between the rollers and the preform, ensuring that the deformation mechanics remain unchanged. Holding the preform stationary, avoids the need to model the rotational dynamics of the meshed domain, which is computationally intensive.

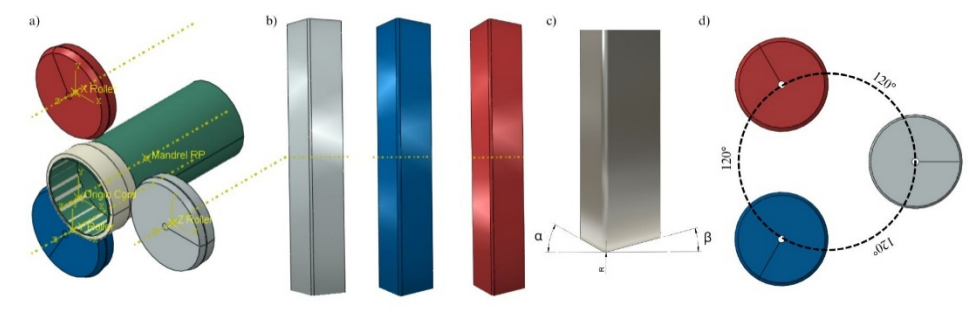


Fig. 1: a) Isometric View of flow-forming setup, b) Roller Geometry, c) Schematic diagram of Roller geometry & d)

Circumferential Stagger given for rollers in the setup

This study investigates the thermo-mechanical behaviour of three different materials—MDN 250, 15CDV6, and AISI 4130 which are commonly used in aerospace and defence applications. MDN 250 is maraging steel, known for its ultra-high strength, excellent fracture toughness, and minimal distortion after heat treatment, making it suitable for applications such as rocket motor casings, pressure vessels, and aircraft landing gear. 15CDV6, which is a chromium-molybdenum-vanadium alloyed steel, offers a high strength-to-weight ratio, good weldability, and outstanding toughness, which are advantageous for critical structural components like fuselage frames, landing gears, and fasteners. On the other hand, AISI 4130 is a low-alloy steel, which is widely used in the fabrication of rocket motor tubes and pressure vessels due to its balanced combination of strength, fatigue resistance, and ductility. The material behaviour in the model is defined using the Johnson–Cook (JC) constitutive model, incorporating strain, strain-rate, and thermal softening effects. The JC model parameters for each material are obtained from existing literature [9], [10], [11].

The contact interactions between the roller and preform, as well as between the preform and the mandrel, are defined using surface-to-surface contact formulations instead of general contact, to enhance the accuracy and stability of the contact algorithm. A coefficient of friction of 0.1 is considered as per literature [9]. The preform is initialized at room temperature to represent ambient conditions.

In this study, the input parameters selected for the analysis are - feed ratio, percentage reduction, and axial stagger. Corresponding output responses such as ovality, diametral growth, and spring-back are evaluated to assess the structural integrity of the formed tubes. A Taguchi L9 orthogonal array is employed to design the experiment, resulting in a total of nine simulation trials per material [12], [13]. The design matrix is presented in Table 1.

Simulation Runs Feed Ratio (mm/rev) Percentage Reduction (%) Axial Stagger (mm) 0.75 6.5 - 13.035 2 0.75 50 8.5 - 17.03 0.75 65 10.5 - 21.08.5 - 17.04 1.25 35 50 10.5 - 21.05 1.25 65 6.5 - 13.01.25

35

50

65

10.5 - 21.0

6.5 - 138.5 - 17.0

1.75

1.75

1.75

Table 1: Design of Experiments Table (common for all the three materials).

3. Model Benchmarking

7

8

To validate the model, the thickness obtained from the numerical simulation is compared with the experimental thickness from the reference paper as shown in Figure 2a. The error percentage was found to be 0.52%, therefore it can be considered to be validated.

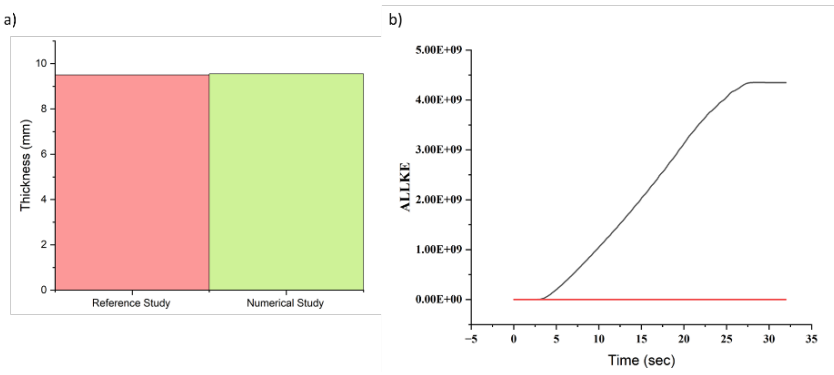


Fig. 2: a) Thickness Comparison b) Energy history plot

To improve computational efficiency in the explicit dynamic simulation, mass scaling was employed with a scaling factor of 10,000. Mass scaling artificially increases the density of elements to allow for larger stable time increments, thereby significantly reducing the overall simulation time [14]. However, excessive mass scaling can compromise the physical accuracy of the results by introducing inertial effects that are not representative of the actual process. To ensure the reliability of the simulation, the ratio of kinetic energy (ALLKE) to internal energy (ALLIE) was monitored throughout the analysis. This ratio is a critical indicator of numerical stability and physical realism; it is generally recommended to keep ALLKE/ALLIE below 5% to confirm that inertial effects do not dominate the material response. In the present study, despite the high mass scaling factor, the energy ratio remained well within acceptable limits, with a maximum observed percentage is 0.006730 %, ensuring the simulation results are both efficient and physically meaningful. The energy history plot of one simulation is shown below in Figure 2b.

4. Results and Discussions

4.1. Effective Stress and Equivalent Plastic Strain (PEEQ) Distribution

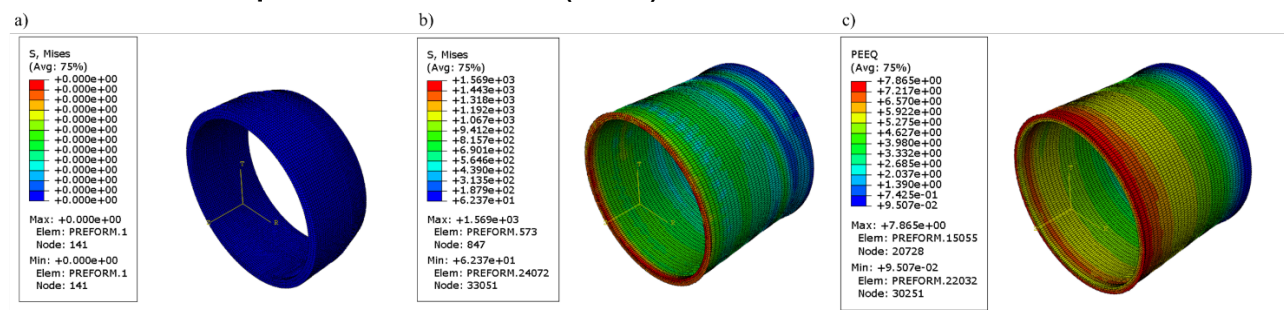


Fig. 3: Contour Plots a) Preform, b) Effective stress of flow-formed tube, c) PEEQ of flow formed tube

Figure 3 shows the distribution of effective stress (von Mises) and equivalent plastic strain (PEEQ) for Case 9 from the DOE table (15CDV6), corresponding to a 65% reduction. The yield stress of 15CDV6 is 790 MPa and the ultimate tensile strength (UTS) is typically around 1000 – 1200 MPa. Figure 3a depicts the initial preform geometry. In Figure 3b, the effective stress reaches a maximum of 1566 MPa, which is well above the yield point and UTS, clearly indicating that the material has undergone plastic yielding and softening. This allows the material to enter fully under plastic deformation regime and allows the material to flow. The high-stress regions are concentrated near the roller–workpiece interface, highlighting the localized nature of plastic flow during forming. The PEEQ contour in Figure 3c further confirms this, showing peak values up to 7.86, which is characteristic of a high-strain forming process. The higher strain distribution along the retreating end is indicative of the rollers which just passed by from the region.

4.2. Influence of Process-parameters on Output Parameters

The influence of key flow-forming parameters on the geometric accuracy of MDN-250, 15CDV6, and AISI 4130 was evaluated using Taguchi L9 Orthogonal design. The output responses like ovality, diametral growth and spring-back, PEEQ, and temperature were analysed based on the main effective plots as shown in Figures 4, 5, 6, 7, and 8.

4.2.1. Ovality

From the above results it was observed that the percentage reduction emerges as the most dominant contributor compared to other process parameters. For all the metals, increasing percentage reduction to 65% significantly elevated the ovality values, indicating distortion of the circular profile due to excessive plastic flow. For MDN-250 from figure 4a, a relatively moderate ovality was observed at lower reduction, while 15CDV6 (figure 4b) showed a marginally lower value. On the other hand, AISI 4130 (figure 4c) exhibited the highest peak in ovality on higher feed rates and reduction combinations, suggesting to its lower resistance to deformation under these conditions. At higher feed ratios the rollers

advance more rapidly along the axial direction, reducing the contact time per revolution and thereby reducing the circumferential flow. This is also evident from the reduced effective plastic strain shown in Figures 7a -7c. This can result in incomplete deformation and less material conformance, leading to ovality which can be clearly observed in AISI 4130 (Figure 4c) and 15CDV6 (Figure 4b). Conversely, lower feed rates allow for slower, more controlled deformation enabling the rollers to better shape the preform and promote uniform circumferential flow, thereby reducing ovality.

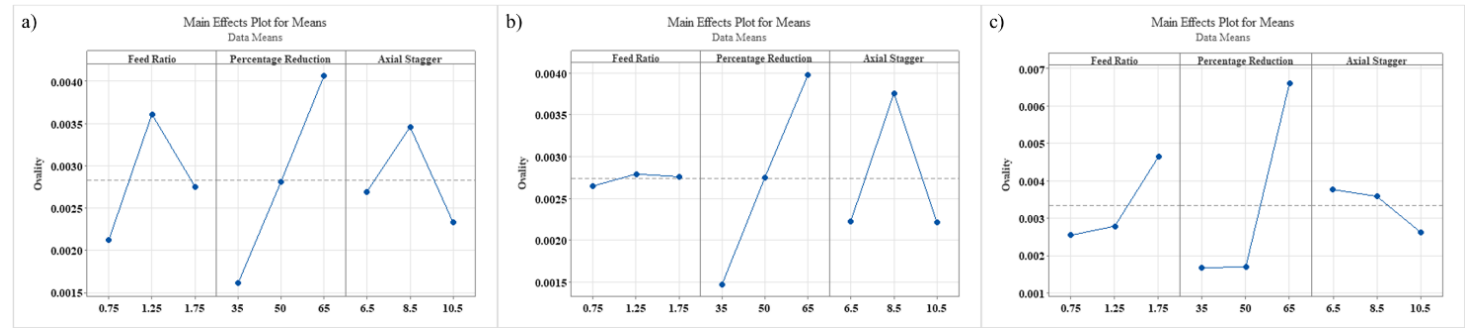


Fig. 4: Main Effective Plots for ovality on a) MDN-250, b)15CDV6, c) AISI 4130

Axial stagger showed a mild influence with a reduced ovality at higher stagger conditions. The material has more time and space to relax and redistribute stress before engagement by the next roller. This helps to minimize the accumulation of residual circumferential strain and results in better ovality as seen in figure 4a, 4b and 4c respectively. In contrast smaller stagger distances can cause the rollers to engage the preform in quick successions, offering less time for the material to stabilize between deformations. This may lead to localized stress build-up and amplify non-uniform flow thereby increasing ovality. Interestingly, 15CDV6 and MDN-250 showed a deviation with peak ovality at a medium stagger. This suggests a possible interaction between its material characteristics (like strain hardening and strain-rate sensitivity) and the staggered rollers engagement, leading to insufficient stress distribution at the intermediate distances.

4.2.2. Diametral Growth

Diametral Growth trends indicate strong correlation with percentage reduction, consistent across all the materials. In all the cases, higher reduction levels (65%) led to the maximum diametral growth, which is expected due to radial thinning and outward material flow, often resembling bell-mouthing near the tube ends. Among the materials, 15CDV6 shown in Figure 5b displayed the highest diametral growth, followed by MDN-250 (Figure 5a) and AISI 4130 (Figure 5c). This suggest that 15CDV6 is more prone to radial expansion under aggressive deformations, possibly due to its strain hardening exponent. On the other hand, MDN-250 despite it having a lower strain hardening exponent, showed a better containment due to higher base flow stress. This is because, even though MDN-250 doesn't strain harden much it has a higher yield strength which makes it intrinsically stronger and more resistant to plastic deformation from the beginning.

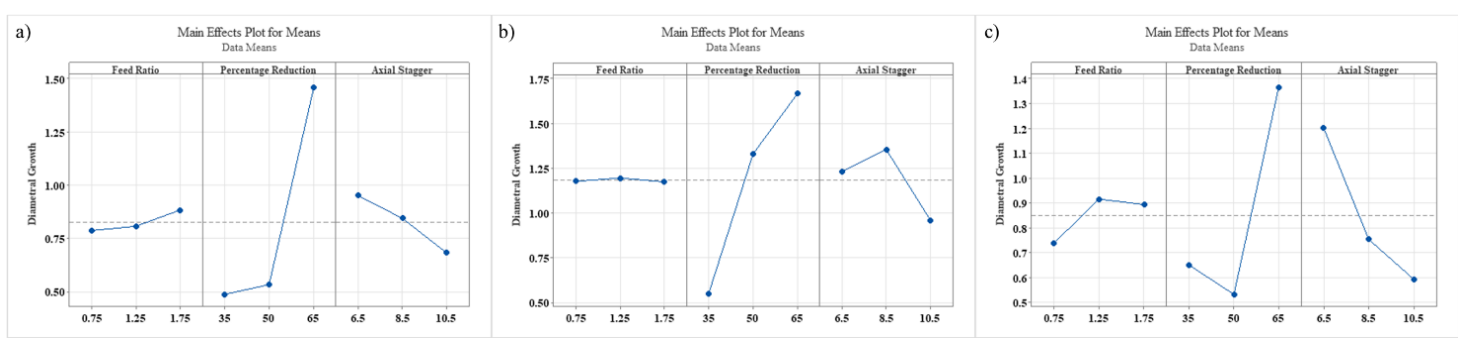


Fig. 5: Main Effective Plots for diametral growth on a) MDN-250, b)15CDV6, c) AISI 4130

Feed ratio exhibited minimal influence on diametral growth for 15CDV6 and AISI 4130, while MDN-250 showed a slight upward trend with increased feed, indicative of a reduced roller engagement with the material which leads to insufficient material flow along the radial direction, increasing the diametral growth. For all the materials, increasing axial stagger effectively reduced diametral growth, most noticeable in AISI 4130 where a sharp drop from lower stagger to higher stagger indicates enhanced stress redistribution and reduced radial expansion between the staggered roller passes.

Interestingly, these diametral growth patterns closely mirror the trends observed in ovality. Both responses are affected by non-uniform material flow and roller engagement dynamics, particularly at higher percentage reductions and feed ratios. While ovality captures the circumferential asymmetricity, diametral growth reflects the bulk radial expansion. Yet both are strongly driven by how effectively the material conforms to the mandrel during deformation. The common trend emphasizes the importance of controlling feed rate and maintaining optimal stagger spacing to achieve dimensional stability and reduce geometrical distortions.

4.2.3. Spring-Back

Spring-back exhibited a trend closely aligned with diametral growth, with percentage reduction as the most dominating influential factor across all materials. As the reduction increased to 65%, all the specimens displaced a notable rise in spring-back, which can be attributed to the greater accumulation of elastic strain energy during plastic deformations. When the forming load is removed this stored energy is released, causing the material to recover partially and return to its final intended shape. Among the three materials, AISI 4130 recorded the highest spring-back, reaching values near 0.95 mm (Figure 6c). This is consistent with its lower yield strength and relatively higher elastic modulus, which together favour a stronger elastic recovery post-deformation. In contrast MDN-250, exhibited the lowest spring-back (Figure 6a), owing to its higher flow-stress and thermal resistance, which helped in maintaining dimensional stability even under significant plastic loading.

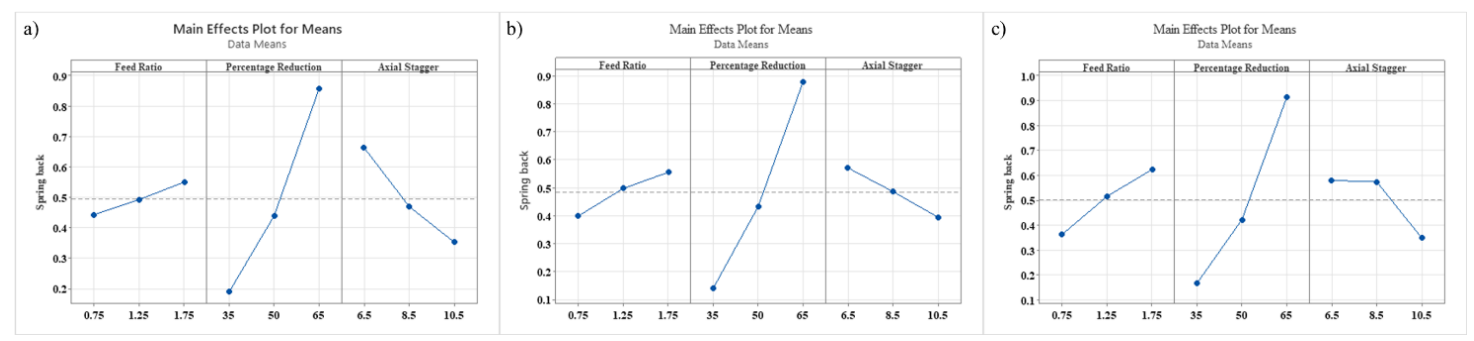


Fig. 6: Main Effective Plots for spring-back on a) MDN-250, b)15CDV6, c) AISI 4130

The influence of feed ratio on spring-back was moderate but consistent. Higher feed rations tend to induce more spring-back in all materials. This can be explained by reduced roller engagement per revolution at higher feed rate, leading to less uniform plastic deformations and higher residual stress concentrations, especially near the surface layers.

Axial stagger had a clear beneficial effect on minimizing spring-back. As the axial distance between the rollers increased, the material experienced more distributed and sequential deformation, allowing for partial stress relaxation between roller engagements. This reduced the net elastic recovery upon unloading, particularly in AISI 4130, which showed a marked drop in spring-back at higher stagger values. The effectiveness of staggered roller engagement in breaking up localized strain zones highlights its role in smoothing residual stress gradients thereby enhancing post-forming dimensional accuracy.

4.2.4. Equivalent Plastic Strain

The equivalent plastic strain (PEEQ) serves as a key indicator of the total plastic deformation experienced by the material during flow-forming. Across all the three materials, the percentage reduction has emerged as the most dominant parameter

influencing PEEQ. As shown in Figures 7a-7c, increasing the percentage reduction from 35% to 65% led to a sharp increase in PEEQ values. This is expected since higher reduction forces leads to more material flow, which causes greater accumulation of plastic strain.

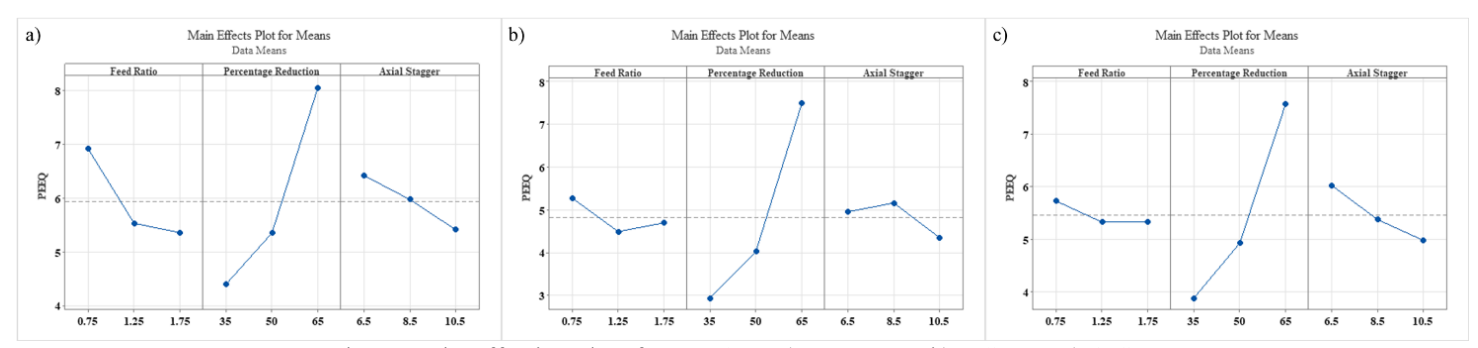


Fig. 7: Main Effective Plots for PEEQ on a) MDN-250, b)15CDV6, c) AISI 4130

MDN-250 exhibited the highest PEEQ at 65% reduction, indicating greater plastic strain accumulation under severe forming conditions. This can be correlated to its low strain hardening exponent (n), which allows the material to plastically deform easily after yielding, with minimal increase in resistance. 15CDV6 and AISI 4130 showed slightly lower PEEQ magnitudes, likely due to their relatively higher n value which provides more resistance to progressive strain buildup.

The feed ratio showed a relatively moderate but consistent trend. At lower feed ratios, all the materials experienced a slightly higher value. This is attributed to prolonged roller contact at each axial location, allowing more uniform and extensive plastic strain. Axial Stagger also influences PEEQ across all the material. A trend of slightly decreasing PEEQ with increasing stagger was observed. This can be explained by the increased spacing between the rollers allowing intermediate stress relaxations and smoother plastic flow.

4.2.5. Temperature

The temperature developed during the flow-forming process is a result of plastic deformation work and frictional heating at the roller workpiece interaction. To understand the temperature evolution at the roller-workpiece interface, a representative simulation was analysed, specifically, Case 9 for 15CDV6 material with 65% reduction, where high plastic deformation is expected. A nodal temperature history was plotted from a point located directly beneath the roller contact zone as shown in Figure 8. The graph shows a sharp rise in temperature as the roller approaches and passes over the node (at 14.43 seconds), peaking at approximately 610 K. following by gradual stabilization. This behaviour confirms that the maximum thermal accumulation consistently occurs in the roller contact region due to intense plastic work and frictional heating. Since similar thermal localization was observed across all the simulation cases, this representative example effectively illustrates the temperature profile associated with severe deformation conditions.

All the three materials, percentage reduction was the most dominant factor influencing temperature rise. As seen in Figure 9a -9c, increasing the reduction from 35% to 65% led to a steep increase in temperature, which is expected due to the significant increase in deformation energy and strain rate reductions. Among the materials, 15CDV6 showed the highest peak temperatures, reaching up to 330 K at 65% reduction followed by MDN-250 and AISI 4130. Interestingly, despite having a lower thermal softening exponent, 15CDV6 exhibited the greatest thermal build-up. This indicates that the material retains much of its strength even at elevated temperatures, resulting in sustained plastic deformation and greater heat generation. On the other hand, MDN-250 and AISI 4130 with higher thermal softening exponents, exhibits more significant strength degradation as temperature rises, which could result in localised material softening and stress distribution. Since feed ratio is defined as the axial feed per mandrel revolution, it directly controls the interaction time and deformation intensity between the roller and workpiece. At higher feed ratios, the roller moves faster along the axis, reducing contact time per unit area but still forcing significant plastic deformation (roller forces). This leads to higher strain rates and more localized energy input, resulting in a greater temperature rise. In contrast, lower feed ratios involve slower roller advancement, allowing more time

per unit area for deformation to occur. This produces lower strain rates, more uniform plastic flow, and consequently lower heat generation, resulting in a more moderate temperature increase.

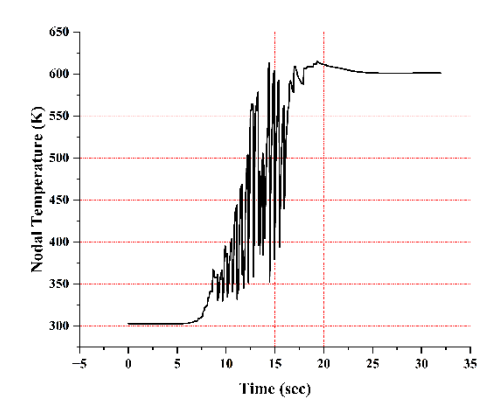


Fig. 8: Nodal temperature history plot

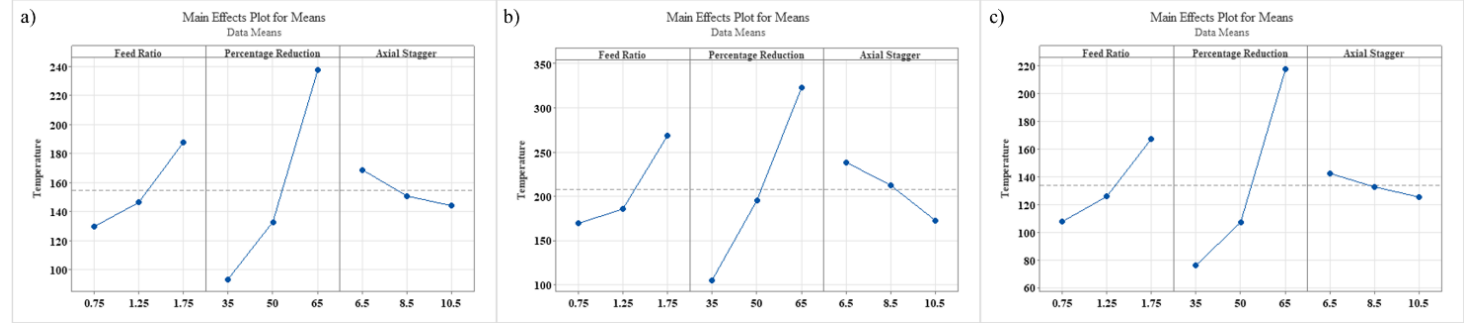


Fig. 9: Main Effective Plots for Temperature on a) MDN-250, b)15CDV6, c) AISI 4130

Increasing the stagger distance allowed more thermal relaxation time between successive roller passes. This helped to mitigate the cumulative heat generation, especially in 15CDV6 and AISI 4130, where temperature dropped notably at higher staggers. For MDN-250, the trend was similar but less steep, likely due to its higher resistance to plastic strain and efficient softening behaviour at elevated temperatures.

5. Conclusion

This study systematically investigated the influence of feed ratio, percentage reduction, and axial stagger on geometric and thermal responses in the flow forming of MDN 250, 15CDV6, and AISI 4130 using a Taguchi L9 design. Among the input parameters, percentage reduction consistently emerged as the most dominant factor, as it directly governs the extent of plastic deformation and associated heat generation, thereby significantly affecting ovality, diametral growth, spring-back, PEEQ, and temperature rise. Higher feed ratios led to increased geometric deviations and temperature rise due to reduced roller contact time per unit area at elevated strain rates. In contrast, greater axial stagger effectively mitigated ovality, spring-back, and temperature accumulation by promoting better stress redistribution and allowing partial thermal relaxation between roller passes. These findings provide useful insights for analysing flow-forming process parameters to achieve enhanced dimensional accuracy and thermal stability. From the research we can conclude that the ideal condition would lower feed rates, lower to moderate percentage reduction and higher axial stagger can lead to better dimensional accuracy and structural integrity of the flow-formed tubes.

References

[4]

[5]

- [1] D. Marini, D. Cunningham, and J. Corney, "A review of flow forming processes and mechanisms," *Key Eng Mater*, vol. 651–653, pp. 750–758, 2015, doi: 10.4028/WWW.SCIENTIFIC.NET/KEM.651-653.750.
- [2] C. C. Wong, T. A. Dean, and J. Lin, "A review of spinning, shear forming and flow forming processes," *Int J Mach Tools Manuf*, vol. 43, no. 14, pp. 1419–1435, 2003, doi: 10.1016/S0890-6955(03)00172-X.
- [3] O. Music, J. M. Allwood, and K. Kawai, "A review of the mechanics of metal spinning," Jan. 01, 2010. doi: 10.1016/j.jmatprotec.2009.08.021.
 - N. A. Razani, A. Jalali Aghchai, and B. Mollaei Dariani, "Experimental study on flow forming process of AISI 321 steel tube using the Taguchi method," *Proc Inst Mech Eng B J Eng Manuf*, vol. 225, no. 11, pp. 2024–2031, Nov. 2011, doi: 10.1177/0954405411398195.
 - M. Srinivasulu, M. Komaraiah, C. S. Krishna, and P. Rao, "Experimental investigations to predict mean diameter of AA6082 tube in flow forming process-A DOE approach," *IOSR Journal of Engineering (IOSRJEN)*, vol. 2, no. 6, pp. 52–60, 2012, Accessed: Jun. 14, 2025. [Online]. Available: www.iosrjen.org
- [6] M. H. Parsa, A. M. A. Pazooki, and M. Nili Ahmadabadi, "Flow-forming and flow formability simulation," *International Journal of Advanced Manufacturing Technology*, vol. 42, no. 5–6, pp. 463–473, May 2009, doi: 10.1007/S00170-008-1624-0/METRICS.
- [7] M. Haridas, G. Gopal, A. Ramesh, and R. Kumar Katta, "Modelling and simulation of single and multi-pass flow forming to investigate the influence of process parameters on part accuracy," 2016.
- [8] K. M. Rajan, P. U. Deshpande, and K. Narasimhan, "Effect of heat treatment of preform on the mechanical properties of flow formed AISI 4130 Steel Tubes—a theoretical and experimental assessment," *J Mater Process Technol*, vol. 125–126, pp. 503–511, Sep. 2002, doi: 10.1016/S0924-0136(02)00305-9.
- [9] H. Shinde, P. Mahajan, A. K. Singh, R. Singh, and K. Narasimhan, "Process modeling and optimization of the staggered backward flow forming process of maraging steel via finite element simulations," *International Journal of Advanced Manufacturing Technology*, vol. 87, no. 5–8, pp. 1851–1864, Nov. 2016, doi: 10.1007/s00170-016-8559-7.
- [10] A. Padmakumar, A. P. Madhavan, J. Joseph, and S. Kailasamani, "Transient Thermal Analysis on Rotary Friction Welding of 15CDV6 Aerospace Steel," *Transactions of the Indian Institute of Metals*, vol. 76, no. 3, pp. 799–808, Mar. 2023, doi: 10.1007/s12666-022-02759-3.
- [11] L. Wuertemberger and A. N. Palazotto, "Evaluation of Flow and Failure Properties of Treated 4130 Steel," *Journal of Dynamic Behavior of Materials*, vol. 2, no. 2, pp. 207–222, Jun. 2016, doi: 10.1007/S40870-016-0059-1/TABLES/7.
- [12] B. Durakovic and K. Prakash Marimuthu, "Minimization of Milling-Induced Residual Stresses in AISI 1045 Steel: Process Optimization using Design of Experiments Taguchi Method," *J Mater Eng Perform*, vol. 33, no. 15, pp. 7721–7727, Aug. 2024, doi: 10.1007/S11665-024-09570-9/FIGURES/4.
- [13] G. S. Kailash, B. M. Reddy, D. Gugulla, M. S. Chouhan, and M. Prashanth, "Milling of D3 Tool Steel to Optimize Machining Parameters and Develop a Mathematical Model to Achieve Minimum Surface Roughness," *AIP Conf Proc*, vol. 2943, no. 1, Dec. 2023, doi: 10.1063/5.0183314.
- [14] S. B. T. Surendran, C. S. Sumesh, and A. Ramesh, "Numerical Modeling of Orthogonal Machining Process Using Smoothed Particle Hydrodynamics—A Parametric Study," *Lecture Notes in Mechanical Engineering*, pp. 497–509, 2021, doi: 10.1007/978-981-15-4745-4_44/FIGURES/7.